Forecasting the North African dust outbreak towards Europe in April 2011: A model intercomparison

N. Huneeus[1,2], S. Basart[3], S. Fiedler[4,5*], J.-J. Morcrette[6], A. Benedetti[6], J. Mulcahy[7], E. Terradellas[8], C. Pérez García-Pando[9,10], G. Pejanovic[11], S. Nickovic[11,12], P. Arsenovic[11,13], M. Schulz[14], E. Cuevas[15], J.M. Baldasano[3,16], J. Pey[12,17], S. Remy[6#], B. Cvetkovic[11]

[1]{Laboratoire de Météorologie Dynamique, IPSL, CNRS/UPMC, Paris, France}

[2]{Department of Geophysics and Center for Climate and Resilience Research, University of Chile, Santiago, Chile}

[3]{Earth Sciences Department, Barcelona Supercomputing Center, BSC-CNS, Barcelona, Spain}

[4]{School of Earth and Environment, University of Leeds, Leeds, UK,

[5]{Institute of Meteorology and Climate Research, Institute of Technology, Karlsruhe, Germany}

[6]{European Centre for Medium-Range Weather Forecasts, Reading, UK}

[7]{Met Office, FitzRoy Road, Exeter, EX1 3PB, UK}

[8]{Meteorological State Agency of Spain (AEMET), Barcelona, Spain}

[9]{NASA Goddard Institute for Space Studies, New York, USA}

[10]{Department of Applied Physics and Applied Math, Columbia University, New York, USA}

[11]{National Hydrometeorological Service, Belgrade, Serbia}

[12]{Institute of Environmental Assessment and Water Research, Spanish Research Council, Barcelona, Spain}

[13]{Institute for Atmospheric and Climate Science, ETH, Zürich, Switzerland}

[14]{Norwegian Meteorological Institute, Oslo, Norway}

[15]{Izaña Atmospheric Research Center, State Meteorological Agency of Spain (AEMET),

Santa Cruz de Tenerife, Spain}
[16]{Environmental Modelling Laboratory, Technical University of Catalonia, Barcelona, Spain}
[17]{Geological Survey of Spain (IGME), Zaragoza, Spain}
[*]{Now at Max-Planck Institute for Meteorology, Hamburg, Germany}
[#]{Now at Laboratoire de Météorologie Dynamique, IPSL, CNRS/UPMC, Paris, France}
Correspondence to: N. Huneeus, nhuneeus@dgf.uchile.cl

Abstract

In the framework of the World Meteorological Organisation's Sand and Dust Storm Warning Advisory and Assessment System, we evaluated the predictions of five state-of-the-art dust forecast models during an intense Saharan dust outbreak affecting Western and Northern Europe in April 2011. We assessed the capacity of the models to predict the evolution of the dust cloud with lead-times of up to 72 hours using observations of aerosol optical depth (AOD) from the Aerosol Robotic Network (AERONET) and the Moderate Resolution Imaging Spectroradiometer (MODIS), and dust surface concentrations from a ground-based measurement network. In addition, the predicted vertical dust distribution was evaluated with vertical extinction profiles from the Cloud and Aerosol Lidar with Orthogonal Polarization (CALIOP). To assess the diversity in forecast capability among the models, the analysis was extended to wind field (both surface and profile), synoptic conditions, emissions and deposition fluxes. Models predict the onset and evolution of the AOD for all analysed lead-times. On average, differences among the models are larger than differences among lead-times for each individual model. In spite of large differences in emission and deposition, the models present comparable skill for AOD. In general, models are better in predicting AOD than near-surface dust concentration over the Iberian Peninsula. Models tend to underestimate

the long-range transport towards Northern Europe. Our analysis suggests that this is partly due to difficulties in simulating the vertical distribution dust and horizontal wind. Differences in the size distribution and wet scavenging efficiency may also account for model diversity in long-range transport.

1 Introduction

Desert dust, the largest contributor to the global aerosol burden after sea salt (*Textor et al.*, 2006; *Huneeus et al.*, 2013), plays an important role in the climate system, the chemical composition of the atmosphere (e.g. *Sokolik et al.*, 2001; *Tege*n, 2003; *Balkanski et al.*, 2007; *Bauer and Koc*h, 2005) and the ocean biogeochemical cycles (*Jickells et al.*, 2005; *Aumont et al.*, 2008, *Mahowald et al.*, 2009; *Schulz et al.*, 2012; *Gallisai et al.*, 2014). Besides their climate effect, dust aerosols degrade air quality over large regions of the globe (e.g. *Kim et al.*, 2001; *Ozer et al.*, 2007; *Querol et al.*, 2009; *Pey et al.*, 2013) and often disproportionately reduce visibility close to source regions, impacting transportation (road vehicles and airports), military operations and photovoltaic energy production (e.g. *Schroedter-Homscheidt et al.*, 2013). Some evidence exists for increased mortality when dust aerosols are present in particulate matter with radius smaller than 10 μm (PM10) (*Jiménez et al.*, 2010; *Karanasiou et al.*, 2012), and dust storms have been associated to epidemics of meningococcal meningitis in the African Sahel (*Agier et al.*, 2013; *Pérez García-Pando et al.*, 2014a,b).

The wide variety of impacts along with the importance of dust for weather forecasting (*Pérez et al.*, 2006a) have motivated the development of operational forecasting capabilities to predict the occurrence of dust storms (*Benedetti et al.*, 2014). Moreover, the European Union directives establish that model results can be used to determine whether PM10 exceedances are caused by advection of dust or by local pollution. Considering the financial implications of this, there is motivation for atmospheric composition forecast models to improve their performance related to dust. At present, a number of global and regional dust forecast systems are available (e.g. *Woodwar*d, 2001; *Morcrette et al.*, 2008; 2009; *Pérez et al.*, 2011; *Basart et al.*, 2012; *Zhou et al.*, 2008; *Vogel et al.*, 2009). An important limitation for the advancement of operational dust storm forecasts is the lack of standardized evaluation processes, suitable observations and a poorly developed verification system compared to numerical weather prediction (NWP). While NWP benefits from advanced near-real time observations systems and well-established protocols for the evaluation of forecast products, similar procedures for aerosol forecasting are at their beginning (*Reid et al.*, 2010; 2011).

Recently two international programs for model intercomparison and observation of dust storms emerged: the Sand and Dust Storm Warning Advisory and Assessment System (SDS-WAS) led by the World Meteorological Organization (WMO, http://www.wmo.int/sdswas) and the International Cooperative for Aerosol Prediction (ICAP) initiative (http://icap.atmos.und.edu/). The SDS-WAS seeks to achieve a comprehensive, coordinated and sustained observations and modelling capacity for sand and dust storms (*Terradellas et al.*, 2013). The overall aims are the monitoring of these events, increase the understanding of the dust processes and enhance the dust prediction capabilities. SDS-WAS is organized around two regional nodes, managed by Regional Centres (RC), namely the Northern Africa-Middle East-Europe Regional Centre (NAMEE) hosted by Spain (http://sds-was.aemet.es/), and the Asian Regional Centre hosted by China (http://www.sds.cma.gov.cn/). Each one of these nodes focuses on sand and dust storms within their region of action. More recently the ICAP (http://icap.atmos.und.edu/) was started. This international forum involves multiple centres delivering global aerosol forecast products and seeks to respond to specific needs related to global aerosol forecast evaluation (*Benedetti et al*., 2011). In contrast to SDS-WAS, this cooperative does not focus exclusively on dust but investigates forecast capabilities of all aerosol species at the global scale. Dust prediction is, however, an important component of the aerosol prediction activities.

Multiple studies have evaluated the model performance to simulate a given dust event (e.g. *Pérez et al*., 2006b; *Heinold et al*., 2007; *Guerrero-Rascado et al*., 2009; *Kalenderski et al*., 2013), yet only a few have analyzed in detail the model capabilities to predict them up to a few days ahead. *Alpert et al*. (2002) use the aerosol index (AI) of the Total Ozone Mapping Spectrometer (TOMS) to initialize a dust prediction system over Israel developed in the framework of the Mediterranean-Israeli Dust Experiment (MEIDEX). *Zhou et al*. (2008) evaluate an operational sand and dust storm forecasting system (CUACE/Dust) for East Asia, while *Shao et al*. (2003) present a real-time prediction system of dust storms in Northeast Asia. These forecasts successfully predict the temporal and spatial evolution of the dust plume, but little effort has been made to systematically examine the predictability of dust transport from Northern Africa to Europe.

The present work is done within the framework of the SDS-WAS NAMEE node. This RC gathers and coordinates the exchange of forecasts produced by different dust models and conducts regular model inter-comparison and evaluation within its geographical scope. We examine the performance of five state-of-the-art dust forecast models to predict the intense Saharan dust outbreak transporting dust over Western Europe to Scandinavia between 5 and 11 April 2011. Studying a single dust event allows to investigate the model skill in predicting the approach of a dust event with a high temporal resolution of a few hours. Each model is compared against a set of observations, namely dust surface concentration, extinction profiles, aerosol optical depth (AOD) at 550 nm, wind at 10 m above ground level (a.g.l.) and profiles of the horizontal wind. This comprehensive inter-comparison of the models reveals strengths and weaknesses of individual dust forecasting systems and provides an assessment of uncertainties in simulating the atmospheric dust cycle at high temporal resolution. The paper is structured as follows. In Sect. 2 the observational data used for the evaluation and the models considered in this work are introduced. In Sect. 3 we describe the intense dust event selected for this study. Results are shown in Sect. 4 and their discussion is provided in Sect. 5. Our conclusions are described in Sect. 6.

2 Data and models

The model evaluation focuses on the days of the event, i.e. from the 5 to 11 of April, and uses data over the North African source region and Europe. Figure 1 shows the region of study along with the locations of the observation stations used. The models are evaluated against aerosol optical depth (AOD), vertical profiles of aerosol backscatter and extinction coefficient (Sect. 2.1), dust surface concentrations (Sect. 2.2), wind speed and other meteorological variables relevant for the event (Sec. 2.3). We conduct a statistical analysis, based on 3-hourly data whenever possible and daily data otherwise and we analyse the models' performance to predict the event with lead-times of 24, 48 and 72 hour. A brief description of each of these datasets follows together with a general description of the models used in this work (Sect. 2.4).

2.1 Aerosol remote sensing

We used AOD observations at 550 nm from 21 Sun photometers operating within the AErosol RObotic NETwork (AERONET; *Holben et al.*, 1998) whose locations are depicted in Figure 1. We use quality-assured direct-sun data (Level 2.0) between 440 and 870nm, which contain an uncertainty on the order of 0.01 for AOD under cloud-free conditions.

Quantitative evaluations of the modelled dust AOD are conducted for dust-dominated conditions; i.e when the Angström exponent (AE) is less or equal to 0.75 (Basart et al., 2009). All data with AE larger than 1.2 are associated to fine anthropogenic aerosols and are considered free of dust. Values of AE between 0.75 and 1.2 are associated with mixed aerosols and are not included in the analysis. The AOD at 550 nm is derived from data between 440 and 870 nm following the Ångström's law. Because AERONET data are acquired at 15-min intervals on average, all measurements within ±90 min of the models' outputs are used for the 3-hourly evaluation.

In addition to ground-based observation, we qualitatively compare the modelled dust AOD to satellite-retrieved aerosol distribution from the Moderate Resolution Imaging Spectroradiometer (MODIS) on board the Aqua satellite. We use daily data from the MODIS Level 3 aerosol products from collection 5.1 at 1ºx1º horizontal resolution. The MODIS algorithm over land produces data only for low ground reflectance (i.e. over dark surfaces) leaving dust aerosol over bright deserts undetected (*Remer et al*., 2005). To evaluate the models over deserts we combine the data with the MODIS Aqua Deep Blue product, which provides information over arid and semi-arid areas by employing radiances from the blue channels to enhance the spectral contrast between surface and dust (Hsu et al., 2004; 2006).

In order to examine the predicted vertical profile of dust aerosol, data from the Cloud and Aerosol Lidar with Orthogonal Polarization (CALIOP) sensor on board the Cloud-Aerosol Lidar and Infrared Pathfinder Satellite Observations (CALIPSO) is used. CALIOP is a standard dual-wavelength (532 and 1064 nm) backscatter lidar operating at a polarization channel of 532 nm. It measures high-resolution (1/3 km in the horizontal direction and 30 m in the vertical direction) profiles of the attenuated backscatter of aerosols and clouds at 532 and 1064 nm along with polarized backscatter in the visible channel (*Winker et al*., 2009). We use here the version 3.01 of the Level 2 aerosol backscatter and extinction product at 532 nm (i.e. CAL_LID_L2_05kmAPro-Prov-V3-30). This product has a horizontal resolution of 5 km and a vertical resolution of 60-m in the tropospheric region up to 20 km and 180 m above. We focus on 5 and 7 of April. The model profiles are derived applying a bilinear interpolation to the four closest model grid points to the CALIOP overpass. We also applied a linear temporal interpolation between the two closest 3-hourly outputs to the time of the CALIOP observation.

2.2 Dust surface concentration

We also compare the forecasts against daily surface African dust concentration of PM10 for a number of Southern European regional background (RB) environments. *Pey et al*. (2013) created a database with daily desert dust PM10 concentrations from 2001 to 2011. We use here 24 stations of this dataset (Fig. 1). Daily contributions of African dust to PM10 were obtained by subtracting the daily RB level from the PM10 concentration of the day of the event (*Escudero et al*., 2007). The RB concentration is derived from application of the monthly moving 40th percentile to the PM10 time series after a prior extraction of the days with African dust.

2.3 Wind data

National Meteorological Services operate networks of manned and automated weather stations that regularly report atmospheric conditions following WMO standards. In particular, surface stations report synoptic observations every 3 or 6 hours through the WMO's Global Telecommunications System. These observations, in combination with upper-air soundings, satellites and other remote-sensing products, are the basis to derive the initialization fields for NWP models. We use wind speed and direction at 10 m above ground from 60 stations within the study region and the vertical profiles of horizontal wind from radiosondes launched daily at 12 UTC at Bachar (2.25°W, 31.5°N) in Algeria (Fig. 1).

2.4 Models

The present study uses three regional and two global models that are run in operational forecasting mode at different centres for weather prediction in Europe. The three regional models are BSC-DREAM8b and NMMB/BSC-Dust from the Earth Sciences Department at the Barcelona Supercomputing Center (ES-BSC) and the DREAM8-NMME from the Southeast European Virtual Climate Change Center (SEEVCC) hosted by the Republic Hydrometeorological Service of Serbia. The global models are MetUM^{TM} developed by the UK Met Office and ECMWF/MACC from the European Centre for Medium-Range Weather Forecasts (ECMWF). We evaluated forecasts initialized at 00 UTC with forecast lead-times of 24, 48 and 72 hours using model 3-hourly output fields. The research teams at the modelling centres configured their model experiments independently and not necessarily follow the setup of their respectively daily operational forecast. We clarify that although the modelling systems of SEEVCC and ECMWF include the assimilation of AOD, the simulations conducted by these centres for this study did not include this feature. The spatial resolution, domain size, initial and boundary conditions, differ, in addition to the different physical parameterizations implemented in the models. Details on the individual dust forecasting systems and the model configurations evaluated here are summarized in Table 1. All models provide 3-hourly instantaneous emission fluxes.

In addition to these five models, we use the Modern-Era Retrospective Analysis for Research and Application (MERRA) from the National Aeronautics and Space Administration (NASA; Rienecker et al., 2011) to evaluate the model performance in reproducing the synoptic-scale conditions of the event. Near-surface winds from MERRA are shown for completeness. A discussion of limitations of winds from re-analysis can be found elsewhere (e.g., Menut, 2008; Fiedler et al., 2013, 2015, Largeron et al., 2015).

3 Dust Event

The African dust outbreak affected Europe between 5 and 11 April 2011. On 4 April, an upper level trough approached Northwest Africa from the west. Advection of positive vorticity and the flow interaction with the Atlas Mountains favoured cyclogenesis in the mountain lee (not shown). On 5 of April, the cyclone had deepened over the southern Moroccan-Algerian border causing strong winds of more than 20 ms^{-1} at 850 hPa. The associated near-surface winds produced dust mobilization over Algeria (Fig. 1).

The emitted dust aerosol was subsequently transported northwards and reached the Iberian Peninsula following the cyclonic flow (not shown). On 6 and 7 of April, a ridge of high pressure over France and a cyclone west of the Azores Islands caused south-easterly winds of up to 17 ms^{-1} at 850 hPa to the west of the Iberian Peninsula that advected the dust plume towards the Atlantic Ocean. High pressure built and strengthened over the Iberian Peninsula and Northwest Africa between the 8 and 9 of April. The resulting southerly winds over the Atlantic transported the dust-laden air towards Great Britain. 10 and 11 April were characterized by a ridge over West Europe with strong south-westerly winds over Great Britain, which advected the more diffused dust cloud towards Scandinavia (Fig. 1b).

4 Results

4.1 Dust Transport: AOD and PM10

The northward transport of dust was examined by comparing model AOD forecasts with AERONET measurements at three stations located along the path of the dust cloud (Fig. 2) and daily AOD maps from MODIS (Fig. 3 and Figures S01, S02 and S03 in the Supplement).

The three AERONET stations are Saada (31.63°N, 8.16°W) in Morocco close to the dust source, Evora (38.57°N, 7.91°W) in Portugal, and Birkenes (58.39°N, 8.25°E) in Norway (Fig. 1, black squares). The AOD in Saada peaked on 6 April and a second and smaller maximum was observed on 9-10 April (Fig. 2). The latter peak corresponds to a dust plume that did not affect the Iberian Peninsula and is therefore omitted in our discussion. The time series in Evora and Birkenes feature sharp AOD increases during the passage of the dust cloud (Fig. 2). In Evora, the AOD increased from nearly 0.2 on 5 April to a about 0.8 on the next day. In Birkenes, the AOD raised from approximately 0.3 on 9 April to roughly 1.1 on 10 April (the AOD actually doubled in 10 April between the early morning and the late evening). The dominance of the dust in the AOD is evidenced by the strong decrease of AE to values below 0.6.

The 24-hour forecasts produced by MetUM, ECMWF/MACC and NMMB/BSC-Dust overestimate the AOD on the 5 April in Saada, and, except for ECMWF/MACC, they underestimate the peak on 6 April. While MetUM reproduces the peak on 6 April, NMMB/BSC-Dust predicts it 6 hrs earlier, BSC-DREAM8b and ECMWF/MACC reproduce it 3 hrs earlier. DREAM8-NMME reproduces the AERONET AOD on 5 April but underestimates it on the following day whereas ECMWF/MACC mostly overestimates the AOD on both days. At Evora, most models overestimate the AOD on 6 April with the exception of NMMB/BSC-Dust and DREAM8-NMME. On 7 April MetUM and ECMWF/MACC mostly overestimate the AOD, while the rest of the models tend to underestimate it. The AOD forecast differs significantly for lead-times of 48 and 72-hour. For example, while the 24-hour ECMWF/MACC forecast overestimates the AOD in Saada on 5 and 6 April, the 72-hour forecast mostly underestimates it. Similarly, at Evora, the 24-hour forecast of NMMB/BSC-Dust slightly underestimates the AOD on 6 April whereas the 72-hour forecast markedly overestimates it during the same day. At Birkenes, all models underestimate the AOD on the 10 April regardless of the forecast lead-time, which reflects the models' difficulties to transport dust in high concentrations up north. ECMWF/MACC presents a large spread between the different forecast times. While it features the best performance for the 24 hr forecast, the model skill markedly decreased for the 72 hr forecast.

The maps of daily MODIS AOD (Fig. 3 and Figures S01, S02 and S03 in the Supplement) illustrate the progression of the dust cloud in agreement with the AERONET observations presented above. We note that in order to minimize the potential bias due to temporal sampling associated to the satellite passage, the modelled AOD is computed as the average of the fields at 12 and 15 UTC. The models reproduce the main transport features, but differ in the magnitude of the simulated AOD. While MetUM, ECMWF/MACC and NMMB/BSC-Dust overestimate the magnitude of the AOD suggested by the observations for the first day, the BSC-DREAM8b and DREAM8-NMME underestimates them roughly by a factor of three throughout the entire period. For all models the difference in AOD compared to MODIS increases daily. While MODIS attributes AODs above 1 to the dust cloud until 9 April, the models generally simulate AODs below 1 from the 6 April onwards. BSC- DREAM8b and DREAM8-NMME forecast lower AODs than observed in northern Europe from the 9 April onward. Similar results are found for each model regardless of the forecast lead times, both in terms of spatial features and magnitude of simulated AOD (Figures S02 and S03 in the Supplement).

We used the root mean square error (RMS), mean bias, and Pearson correlation coefficient (R) to assess the skill of each model to predict the AERONET AOD and PM10 (Tables 2 to 6). To explore the performance along the path of the dust cloud, the different AERONET stations were grouped into Southern, Central and Northern Europe (SE, CE and NE, respectively) as indicated in Fig. 1. The models present similar performance between the different lead-times for all regions and all skill scores (Tables 2 to 4). Overall, the largest differences in scores among the models are obtained in NE underlining the growing model spread away from dust sources. However, the scores are not necessarily deteriorated with increasing distance from the source. Although in most cases the models present better statistics in SE, some have better statistics in NE (e.g ECMWF/MACC). In addition, the models present the best RMS and mean bias in CE. Although MetUM has the best AOD performance in SE in terms of all three statistics, there is no model that outperforms the other ones in all regions and for all forecast lead-times.

We examine now the model performance to reproduce near-surface dust concentrations. Most stations in the Iberian Peninsula recorded elevated surface dust concentrations from 6 to 9 April with values between 10 and 100 μg/m^3 (Fig. 4 and Fig. S04 in the Supplement). MetUM strongly overestimates the observations of near-surface concentration for all days and all stations. ECMWF/MACC overestimates the surface concentrations, but captures the variability between 6 and 9 April better, indicating a more realistic development of the dust cloud over Europe. BSC-DREAM8b overestimates the concentrations at southern stations for all days, while an underestimation is found at northern sites during the first half of the event. Finally, NMMB/BSC-Dust and DREAM8-NMME generally tend to underestimate the observed concentrations between 6 and 9 April. The 48 and 72 hr forecast, although different from the 24 hr forecast, show equivalent features to the 24 hr forecast in reproducing the observed surface concentration as described above (Figures S05 and S06 in the Supplement).

The near-surface concentration over the Iberian Peninsula is a critical measure for the dust outbreak and is summarized in Table 5. Overall, the models show similar performance in near-surface concentration of dust aerosols regardless of the forecast lead-times. MetUM presents the largest RMS and mean bias among the models for all lead-times while

DREAM8-NMME presents the smallest bias but also the smallest correlation and NMMB/BSC-Dust features the largest correlation.

4.2 Dust emissions

The atmospheric transport of dust aerosol depends, among other factors, on the amount, time and place of dust emission. In order to give evidence for possible reasons of model differences identified in the previous sections, the spatial and temporal variability of dust emissions from each model at different forecast lead-times between the 4 and 7 April is compared here.

The models present large diversity in both magnitude and spatial distribution of the daily dust emissions within the active source regions (Fig. 5). Except for NMMB/BSC-Dust, with maximum emissions on 4 April, the emissions peak within the region of interest on 5 April and decrease thereafter. The overall largest emissions on 5 April are forecasted by MetUM and the smallest ones by ECMWF/MACC. The large emissions from the former are consistent with the overestimated AOD at Saada on 5 April shown in Figure 2. MetUM is the only model to present similar results for the different forecast lead times (Figure S07 and S08). The remaining models forecast mostly increasing emissions with increasing lead-time for 6 and 7 April. Models ECMWF/MACC and BSC-DREAM8b present both larger emissions for the 72 hr forecast than the 24 and 48 hr forecast on 4 April and vice versa for the following day.

The difference between the largest (MetUM) and the smallest emission (ECMWF/MACC) is of the order of a factor of ten (Fig. 6). This factor is larger than the uncertainty in the annual mean emission from AEROCOM (*Huneeus et al.*, 2011) suggesting that emission uncertainty in single events is particularly large. Most models present maximum emissions on 5 April, except NNMB/BSC-Dust on 4 April. ECMWF/MACC and DREAM8-NMME have emission maxima at 15 UTC whereas MetUM and NNMB/BSC-Dust have the peak in emissions at noon and BSC-DREAM8b at 9 UTC. ECMWF/MACC is the only model with a temporal lag with changing forecast lead-times, namely 3 hrs earlier emissions on 4 April and 3 hrs later on 6 April in the 72 hr forecast. Furthermore, ECMWF/MACC and BSC-DREAM8b have the largest differences between the lead-times; contrary to the 24 and 48 hr forecast, the 72 hr forecast presents the peak in emissions on 4 April and decreasing emissions thereafter. Although the other models also present differences between the forecast lead-times, these are mostly in terms of magnitude, and are smaller compared to emission differences in ECMWF/MACC.

4.3 Vertical dust profiles

The CALIOP observations show for the 5 April a shallow layer concentrating most of the aerosols below 1 km a.g.l. and extending up to 40°N and a second deeper layer between 2 to 9 km a.g.l. and between 25°N and 40°N (Fig. 7). This latter area between 25°N and 40°N coincides with the dust cloud from MODIS as well as the aerosol characterization from the CALIOP product (Fig. S09 in the Supplement). This higher plume can be linked to a precedent dust intrusion that began at the end of March and is not further analysed here. For the 7 April, a deep layer of aerosols extends up to 4 km a.g.l. with most aerosols below two km, south of 25°N and mostly above 2 km between 35°N and 40°N. The latter layer is a consequence of the uplift forced by the Atlas mountains (Fig. S09 in the Supplement).

The models show a large diversity in the 24-hour forecast of extinction coefficient profiles, in particular for the 5 April when the satellite passes over the western margins of the continent and the adjacent Atlantic Ocean. On this day all models simulate a shallow near-surface dust layer over the continent south of 25°N but fail to reproduce the observed northward extension, except the ECMWF model. It shows a dust layer around 1 km a.g.l. but underestimates the intensity. The aerosol layer above 2 km is not simulated by NMMB/BSC-Dust, but visible, with an underestimated depth and height, in the other models. MetUM and ECMWF/MACC limit the vertical extent of the layer to 4 km and show the largest signal centred at 2 km as opposed to 3 km in the observations. Similarly, BSC-DREAM8b and DREAM8-NMME simulate this layer but with even smaller magnitudes.

On the 7 April the models mostly agree on the vertical distribution of the aerosol layer. Except for BSC-DREAM8b, all models represent the aerosol layer mostly confined within the first 2km up to 40°N and the depth of the uplift north of 40ºN is underestimated. BSC-DREAM8b, however, reproduces the depth of the observed layer extending up to 40°N but the depth of the uplift is overestimated and extended to 6 km. Finally, NMMB/BSC-Dust, BSC-DREAM8b and DREAM8-NMME underestimate the observed magnitude of the extinction coefficient, ECMWF/MACC overestimates it, and MetUM simulates values more in agreement with the observations.

4.4 Inter-comparison of synoptic conditions

The synoptic conditions are important for the origin and evolution of the dust cloud. We investigate the model performance to predict the synoptic conditions at mid-day compared to MERRA. Our analysis focuses on the day of dust emission (5 April), transport towards the Atlantic (7 April) and towards Great Britain and Northern Europe (9 April). The inter-comparison of the geopotential height and wind speed analysis at 850 hPa and 500 hPa is shown for each model for the 24 hr forecast in Figures 8 and 9, respectively. The corresponding results for the 48 and 72 hr forecasts are provided in the supplementary material (Figs. S12-S15).

5 April is characterized by a cyclone over the Atlas Mountains in Morocco at 850 hPa and 500 hPa and strong winds around 26 ms^{-1} occurring to the northeast of the cyclone centre at 850 hPa and to the east at 500 hPa (Figs. 8 and 9, respectively). On 7 April the cyclone moved westward while the centre of an anticyclone was located over the Celtic Sea at 850 hPa and near the Pyrenees Mountains at 500 hPa. The associated ridge stretches towards North Africa causing southerlies over the Iberian Peninsula and the Atlantic Ocean. The anticyclone at 850 hPa weakened on 9 April and was located over the North Sea. Similarly the ridge at 500 hPa, although persistent, also weakened and extended from the North Sea to Western Europe.

The 24 hr forecasts reproduced the synoptic development. However, they slightly underestimated the strength of the anticyclone on 7 April at 500 hPa and on 9 April at 850 hPa. ECMWF/MACC, NMMB/BSC-Dust and BSC-DREAM8b also tended to underestimate the anticyclone strength on 7 April at 850 hPa. In addition, BSC-DREAM8b shows larger wind speeds than suggested by MERRA to the west of the cyclone centre in all forecasts, a feature not produced by any other model.

The 48 and 72 hr forecasts do not show major differences compared to the 24 hr forecasts. Some small differences are identified, including an additional weakening of the anticyclone at 850 hPa with increasing lead-time on 5 April in NMMB/BSC-Dust and on 7 April in MetUM. Similarly, the ECMWF/MACC and NMMB/BSC-Dust show a weakening of the ridge at 500 hPa with increasing lead-time. On 7 April, MetUM, NMMB/BSC-Dust and DREAM8-NMME weaken the high pressure at 500 hPa with increasing lead-time while

ECMWF/MACC and BSC-DREAM8b strengthen it. These differences in the strength of the ridge illustrate the model uncertainty in synoptic conditions during the northward transport of the dust cloud. This meteorological uncertainty likely affects the model performance in AOD and surface concentrations. More detailed analysis is needed to reveal the mechanisms causing these differences, which is left for future work.

4.5 Wind analysis

We evaluated the forecasted surface winds, a key driver for dust emission and thereby a potential source for emission differences amongst the models. We used spatial averages of 3-hourly surface wind observations (red dots in Fig. 1) between 4 and 7 April 2011 (Fig. 10). We followed the same procedure with the models and the MERRA reanalysis by averaging the nearest grid cells to the wind observation sites. An in-depth evaluation of winds for dust emission would require an analysis of the wind distributions, which is outside the scope of the present work.

The strongest winds occurred on 4 April, reaching a spatial mean of 5 ms^{-1} at 3 UTC and a south-westerly direction (Fig. 10 and S16 in the supplement material). Peak values in this region were associated to the cyclone in the lee of the Atlas Mountains (Section 2) that caused dust emission. At 6 UTC the wind speed suffered a sharp decrease to 2 ms^{-1} and turned to easterly. The winds are mostly easterly thereafter with a southerly component in the afternoons of 5 and 6 April. The magnitude remains mostly similar from 9 UTC on the 4th until 9 UTC on 5 April, after which winds increased their speed until 21 UTC followed by calms conditions until 12 UTC next day. Calm conditions were also observed during the night of 6 April.

The models initialized 24 hours ahead of the dust event captured the general development of the 10-m wind (Fig. 10); increase of winds on the afternoon of 5 April and decrease on the night of the same day as well as the calm conditions on the night of 6 April. However, except for BSC-DREAM8b, the models mostly overestimate the wind speed throughout the period. Furthermore, the mostly easterly condition of the winds is also captured by all models, but most of them present a stronger meridional (southerly) wind component than the observations in particular on 5 April and most of the next day (Figures S16 and S17 in the supplement material). All models present north-easterly winds at 3 and 6 UTC on 4 April, but BSC-DREAM8b and DREAM8-NMME are the sole models to present northerly wind component from 18 UTC on 4 April until 6 UTC on the next day. Although observations show north-easterly, this only at 6 and 21 UTC on 4 April. Furthermore, no model reproduces the strong winds at 3 UTC on 4 April, neither in terms of magnitude nor in direction. Interestingly, MERRA reanalysis shows similar difficulties to reproduce the observations as the forecasts. Largeron et al. (2015) attributed the overestimation of night-time surface winds of different reanalysis (MERRA one of them) to be linked to overestimation of the turbulent diffusion of the nocturnal dry stable surface layer. This is a common problem of state-of-the-art re-analysis products (Sandu et al., 2013) that can affect dust emission (Fiedler et al., 2013).

We examine now the model performance to forecast the vertical profile of horizontal winds measured by two daily radiosondes (noon and midnight) at Bachar (2.25°W, 31.5°N) in Algeria (Figure 11) close to the dust source of this event (Figure 1). The closest model gridbox to the station is considered in this analysis. Two different regimes can be identified from the observed profiles. The dust-emitting regime until 7 April is characterized by almost constant southerlies above 1 km a.g.l. and easterlies near the surface in agreement with the cyclone (Section 4.4). The wind speeds generally increase until 5 April and decrease thereafter. Maxima in wind speed around 30 m/s on 5 April are reached in two layers centred approximately around 1.5 and 4 km. The subsequent relatively calm regime is characterized by weaker winds and stronger variability in wind direction with height and time. The following analysis will focus on the first regime given its role in the emission and northward transport of dust during the event.

All models simulate the dominant southerlies at elevated levels but they do not reproduce the easterlies close to the surface (Figure 11). Furthermore, most models represent the two maxima in wind speed, yet the maximum around 4 km a.g.l. is weaker and found at higher levels than in the observations. The observed wind maximum between 1 and 2 km a.g.l. is poorly forecasted. Except in ECMWF/MACC, this maximum is forecasted 12 hrs prior to the observations. In addition, the performance to reproduce the depth of the layer with strong winds and its duration varies amongst models. The onset is well reproduced by all models and the strong southerlies agree with observations above 3 km, but below this height, most models terminate the strong winds one day earlier compared to the observations. Lead times of 48 hours show no large impact for the other models (Fig. S19) whereas for lead times of 72 hrs MetUM and BSC-DREAM8b forecast the maximum around 4 km a.g.l. delayed with respect to the observations (Fig. S20).

5 Discussion

The capacity of five models to predict an intense dust event with a lead-time of up to 72 hours was examined. Each model was compared to a set of observations characterizing the dust outbreak from Northwest Africa towards Europe between 5 and 11 April 2011. The focus was to assess the capabilities to predict the evolution of AOD and dust surface concentration along the path of the dust cloud. For the former we compared model outputs to both satellite daily products and ground-based three-hourly observations from the AERONET network whereas for the latter we compared forecasted daily near-surface dust concentration to daily-inferred surface concentration observation. The analysis was extended to wind (both surface and profile), synoptic conditions, aerosol vertical distribution, emissions and deposition fluxes as an attempt to explain the diversity in forecast capability among the models.

Comparison against MODIS AOD revealed that all models reproduce the main features of the daily AOD horizontal distribution throughout the analysed period. However, MetUM, ECMWF/MACC and NMMB/BSC-Dust overestimate the AOD the first days of the event when the dust cloud is over northern Africa and southern Spain, while BSC-DREAM8b and DREAM8-NMME underestimate it. Yet, analysis against AERONET data at Saada, in northern Africa, show that the AOD is mostly underestimated on the days of maximum AOD. We highlight that, according to the simulations, this station is located on the borders of the dust cloud and therefore the bias of each model with respect to the observations is sensitive to both the magnitude of the emitted dust amount and the position of the dust cloud.

We note that while the observed AOD, from both AERONET and MODIS, corresponds to the total AOD and is therefore sensitive to all aerosol species, the simulated one corresponds to the optical depth due to dust particles only. The model bias thus could be partly due to excluded aerosol species. However, the low observed AE (<0.3) on days of maximum AOD (Fig. 2) indicate that the particles in the atmospheric column are dominated by large particles. This is particularly evident at sites remote from dust sources. Furthermore, this allows attributing the model performance in its capacity, at least in days with low AE, to simulate the dust event.

All models agree in underestimating the AOD at Birkenes with respect to both AERONET and MODIS. The underestimation of AOD at Birkenes by models BSC-DREAM8b and DREAM8-NMME is consistent with the underestimation of AOD in northern Africa. However, underestimations by models overestimating the AOD in northern Africa (MetUM, ECMWF/MACC and NMMB/BSC-Dust) suggest that not enough dust is transported northward. This could be associated either to the representation of synoptic conditions affecting the horizontal transport or removal processes in the models.

A difference in emission of the order of a factor of ten is observed between the models (Fig. 6). The individual reasons for the model differences are unknown, but potential sources for differences are discussed in the following. One potential reason for different emission, are the model-dependent emission parameterizations with different particle size distributions. ECMWF/MACC has a size distribution with particles of up to 20 mm in diameter whereas the other four models have maximum sizes of 10 mm (Table 1). However, ECMWF/MACC has the smallest emission. Even for the three models with the same number of bins and the same size distribution (NNMB/BSC-Dust, BSC-DREAM8b and DREAM8-NMME) large emission differences exist pointing to the importance of other aspects. Furthermore, previous studies have shown that dust-emitting winds differ amongst models and can be attributed to the representation of atmospheric processes (e.g., Fiedler et al., 2015). Future studies should examine the detailed differences in winds and size distribution of the emissions, including aspects of model resolution that is crucial to represent different atmospheric processes. Deposition (and its size distribution) should also be examined further in future studies given its importance in model performance to simulate dust concentration and AOD.

Analysis of the total accumulated daily dust deposition suggests that most of the removal occurs in northern Africa close to the source and little is removed over the Atlantic and Europe (Figs. 12 and S21 and S22 in the Supplement). The absence of observed deposition data prevents assessing this aspect of the models performance. The limited deposition away from the source, indicating a too short dust aerosol lifetime in the models, is in agreement with the underestimated dust layer height and AOD away from North Africa. However, observations taken during the Fennec project (Washington et al., 2012) suggest the presence of large particles in higher levels (Allen et al., 2013; Ryder et al., 2013). This could indicate potential dust deposition further away from the source as illustrated by the models and highlights the role of large particles in removal processes as a potential source of errors. It is interesting that the models with the largest emission are not necessarily the ones with the strongest removal, for instance for the first days of the event NMMB/BSC-Dust, BSC-DREAM8b and DREAM8-NMME present stronger total emissions than ECMWF/MACC but lower deposition fluxes.

Comparison of synoptic maps at 850 and 500 hPa of each model against MERRA reanalysis show that models reproduce the main circulation patterns at both levels. Larger differences are observed in the representation of the vertical structure of horizontal wind, in particular the onset and duration of the southerly winds and the height of layers with maximum speed. In addition to this, analysis of the vertical structure of the dust cloud reveals that the models generally underestimate the depth and magnitude of the dust layer as suggested by CALIOP observations. We note however, that CALIOP may overestimate the aerosol extinction coefficient in layers with significant mixture of mineral dust and marine aerosols due to an overestimation of the lidar ratio (*Cuevas et al.*, 2014). Nevertheless, both of the before mentioned factors (vertical structure of horizontal wind and vertical dust propagation) combined could contribute to the reduced northward dust transport to Birkenes in the models;

dust particles do not reach layers of strong winds responsible for the northward transport.

The models show, all in all, similar performance to forecast AERONET AOD. In general no model outperforms the other in all statistics and for both variables (AOD and surface concentration) and the inter-model spread is larger than the change in forecast skill with lead-time. While for the near-surface concentration of dust the NMMB/BSC-Dust presents the best performance in term of all statistics, for AOD the best performing model depends on the region and forecast lead-time. We recall the reader that for analysis with AERONET data, stations were grouped into southern (SE), central (CE) and northern Europe (NE), whereas for surface concentration stations were not grouped but considered as part of southern Europe. Furthermore most models present better RMS and mean bias in CE. This suggests that errors are large both close to dust sources and in long-distance transport. In addition, NE presented in some cases better statistics than SE. The reasons for this has not been examined in detail, but could be a consequence of the low AOD in NE including non-dust situations, i.e. the models successfully reproduce the dust free days in northern Europe. For near-surface dust concentration, the different forecast lead-times also show similar performance for each model. As for AOD, overall the difference between models is larger than the differences between lead-times. We note however that these results correspond to only one event and the number of stations used in this statistical analysis is small (21 stations for AOD and 24 for dust surface concentration) with only a few days considered. Therefore, the statistical significance of these results needs to be explored considering multiple events before drawing generalized conclusions.

We use the mean normalized gross errors (MNGE) to assess the difference between the performance to reproduce AOD and near-surface concentration. This statistic measures the relative difference to the observations and allows comparing two variables with different magnitudes. Consistent with the difficulties of models to reproduce the vertical dust distribution, quantitative assessment of the model performance in AOD and near-surface dust concentration show that models have a better forecast skill for the former independent of the forecasting lead times and station; all show smaller MNGE for the AOD (Table 6). Furthermore, the model diversity to forecast near-surface dust concentration, indicated by the range of MNGE between the models, is much larger than the corresponding range in AOD forecast skill.

In spite of the large model diversity in magnitude and spatial distribution of the emissions and deposition, models present comparable performance when simulating AOD over Northern Africa and Europe. Although this feature can be likely attributed to the practice in model development using AOD values to tune dust simulations, other reasons cannot be excluded. The AOD depends on both, burden and size distribution of dust particles. Therefore, biases in AOD, in particular in the source region, can be associated to biases in the net fluxes and/or to misrepresentation of the size distribution (*Huneeus et al.*, 2011). In addition, definition of optical parameters is also relevant to determine the scattering efficiency of dust particles in a model, and thus AOD. The present study has focused on the forecast skill of the dust lifecycle (i.e. emission, transport and deposition) of a given event from different models, but has not examined the role of size distribution nor definition of optical parameters in the forecast performance.

6 Conclusions

As part of the WMO SDS-WAS five state-of-the-art dust forecast models were examined in their performance to predict an intense Saharan dust outbreak towards Western Europe and Scandinavia between 5 and 11 April 2011. The models are successful in predicting the onset and evolution of the dust cloud in terms of AOD for all three analyzed lead-times, namely 24, 48 and 72 hours. Yet all models underestimate the northward transport of dust, in particular by those models overestimating the AOD in the source region. Weaker horizontal winds, layers with maximum wind at higher altitudes than observed and too shallow dust layers simulated by the models might explain why not enough dust is transported northward. Quantitative forecast-skill analysis revealed that in general no model outperforms the other in all statistics. Nevertheless, the choice of model has a larger impact on the forecast skill than the lead-time. Furthermore, and in agreement with the difficulties to reproduce the vertical distribution of dust, the models perform better in forecasting the AOD in the Iberian Peninsula than the near-surface dust concentrations.

Large diversity exists among the models in their emissions and deposition both in terms of magnitude and spatial distribution. The difference in these fluxes is on the order of a factor ten, exceeding the uncertainty amongst models in the annual mean emission (*Huneeus et al.*, 2011). This result underlines the particularly large model uncertainty for an individual dust storm. In light of the perception that cyclones are reasonably well forecasted, e.g. compared to dust storms due to cold pool outflows from tropical convection (e.g. Heinold et al., 2013), this result is even more striking. The models also present large diversity in the timing of the emissions, varying between afternoon, noon and morning. In spite of these large differences, the models have comparable skills to forecast AOD likely due to the use of AOD values to tune dust models.

The results highlight the need of future studies assessing the performance of dust models to examine individual processes in more detail, particularly the vertical mixing, 3D wind fields, emission/deposition and vertical distribution of dust. These need to be better understood for more robust dust storm forecasting. Emission and deposition need to be further investigated not only in terms of their magnitude but also in terms of spatial distribution. In addition and in spite of the, all in all, successful representation of the synoptic conditions by the different models, the vertical distribution of the horizontal wind and vertical mixing of dust needs to be assessed more extensively. However, we also stress that more observations are needed; the absence of emission and deposition measurements precludes evaluation of the net model fluxes and the current scarcity or lack of routine observations of dust surface concentration, lidar and wind profiles prevent a more detailed assessment of model performance and identifying current sources of bias. Finally, this work has examined the models in their performance for a single event and should be replicated for other events and in other dust source regions before drawing definitive conclusions.

This study has focused on the dust aerosol lifecycle of the event (i.e. emission, transport and deposition) to examine the forecast skill of each model and the differences in skill among them. We have highlighted the importance of the size distribution to conclude on emissions biases due to biases in AOD. However, the impact of the scattering efficiency on the forecast skill has not been addressed. The AOD depends on burden and size distribution, but definition of optical parameters is also relevant to determine the scattering efficiency of dust particles in a model. We suggest that future intercomparison studies examining the model performance to reproduce the dust lifecycle include explicitly the size distribution in their analysis and comparisons against observations allowing to conclude on the performance to reproduce it (e.g. Angström exponent). In addition, the comparison of definition of optical parameters between the different models should also be incorporated.

Acknowledgements

The authors acknowledge AERONET (http://aeronet.gsfc.nasa.gov) and thank the PIs of the AERONET stations used in this paper for maintaining the observation program, and the AERONET-Europe TNA (EU-ACTRIS grant no. 262254) for contributing to calibration efforts. We also acknowledge the MERRA, CALIPSO and MODIS mission scientists and associated NASA personnel for the production of the data used in this research effort. MODIS data used in this paper were produced with the Giovanni online data system, developed and maintained by the NASA GES DISC. S. Basart acknowledge the Catalan Government (BE-DGR-2012) as well as the CICYT project (CGL2010-19652 and CGL2013-46736) and Severo Ochoa (SEV-2011-00067) programme of the Spanish Government. The NMMB/BSC-Dust and BSC-DREAM8b simulations were performed on the MareNostrum supercomputer hosted by BSC. Stephanie Fiedler acknowledges the funding of the European Research Council through the starting grant of Peter Knippertz (Number 257543). Nicolas Huneeus acknowledges FONDAP 15110009. The database on dust concentrations at ground level was produced in the framework of the Grant Agreement LIFE10 ENV/IT/327 from the LIFE Programme of the European Commission. J. Pey has been partially funded by a Ramon y Cajal Grant (RYC-2013-14159) from the Spanish Ministry of Economy and Competitiveness. Carlos Pérez García-Pando acknowledges the Department of Energy (DE-SC0006713), and the NASA Modeling, Analysis and Prediction Program.

Reference

Allen, C. J. T., R. Washington, and S. Engelstaedter (2013), Dust emission and transport mechanisms in the central Sahara: Fennec ground-based observations from Bordj Badji Mokhtar, June 2011, J. Geophys. Res. Atmos., 118, 6212–6232, doi:10.1002/jgrd.50534.

Alpert, P., S. O. Krichak, M. Tsidulko, H. Shafir, and Joseph, J. H.: A Dust Prediction System with TOMS Initialization, *Monthly Weather Review*, *130*(9), 2335-2345, doi=10.1175/1520-0493(2002)130<2335:adpswt>2.0.co;2, 2002.

Aumont, O., L. Bopp, and Schulz, M.: What does temporal variability in aeolian dust deposition contribute to sea-surface iron and chlorophyll distributions?, *Geophys. Res. Lett.*, *35*(7), L07607, doi:10.1029/2007GL031131, 2008.

Bagnold, R. A.: *The Physics of Blown Sand and Desert Dunes* (p. 320). London: Methuen, 1941.

Balkanski, Y., M. Schulz, T. Claquin, and Guibert, S.: Reevaluation of Mineral aerosol radiative forcings suggests a better agreement with satellite and AERONET data, *Atmos. Chem. Phys.*, *7*, 81-95, 2007.

Basart, S., C. Perez, S. Nickovic, E. Cuevas, and Baldasano, J. M.: Development and evaluation of the BSC-DREAM8b dust regional model over Northern Africa, the Mediterranean and the Middle East, *Tellus B*, *64*, doi=Artn 18539Doi 10.3402/Tellusb.V64i0.18539, 2012.

Bauer, S. E., and Koch, D.: Impact of heterogeneous sulfate formation at mineral dust surfaces on aerosol loads and radiative forcing in the Goddard Institute for Space Studies general circulation model, *Journal of Geophysical Research: Atmospheres*, *110*(D17), D17202, doi=10.1029/2005JD005870, 2005.

Benedetti, A., J. S. Reid, and Colarco, P. R.: International Cooperative for Aerosol Prediction Workshop on Aerosol Forecast Verification, *Bull. Amer. Meteorol. Soc.*, *92*(11), ES48-

ES53, doi=10.1175/bams-d-11-00105.1, 2011.

Benedetti, A., J.M. Baldasano, S. Basart, F. Benincasa, O.Boucher, M. Brooks, J.-P. Chen, P.R. Colarco, S. Gong, N. Huneeus, L. Jones, S. Lu, L. Menut, J.-J. Morcrette, J. Mulcahy, S. Nickovic, C. Pérez, J.S. Reid, T.T. Sekiyama, T.Y. Tanaka, E. Terradellas, D.L. Westphal, X.-Y. Zhang, and Zhou, C.-H.: Numerical prediction of dust, in: Mineral dust – a key player in the Earth system, edited by Peter Knippertz and Jan-Berend Stuut, Dordrecht & Springer , 230-240, 2014.

Cuevas, E., Camino, C., Benedetti, A., Basart, S., Terradellas, E., Baldasano, J. M., Morcrette, J.-J., Marticorena, B., Goloub, P., Mortier, A., Berjón, A., Hernández, Y., Gil-Ojeda, M., and Schulz, M.: The MACC-II 2007–2008 reanalysis: atmospheric dust evaluation and characterization over Northern Africa and Middle East, Atmos. Chem. Phys., 15, 3991–4024, doi:10.5194/acp-15-3991-2015, 2015.

Escudero, M., X. Querol, J. Pey, A. Alastuey, N. Pérez, F. Ferreira, S. Alonso, S. Rodríguez, and Cuevas, E.: A methodology for the quantification of the net African dust load in air quality monitoring networks, *Atmospheric Environment*, *41*(26), 5516-5524, doi=http://dx.doi.org/10.1016/j.atmosenv.2007.04.047, 2007.

Fecan, F., B. Marticorena, and Bergametti, G.: Parameterization of the increase of the aeolian erosion threshold wind friction velocity due to soil moisture for arid and semi-arid areas, *Ann. Geophys., 17*(1), 149-157, 1999.

Fiedler, S., K. Schepanski, B. Heinold, P. Knippertz, and I. Tegen, Climatology of nocturnal low-level jets over North Africa and implications for modeling mineral dust emission, J. Geophys. Res. Atmos., 118, 6100–6121, doi:10.1002/jgrd.50394, 2013.

Fiedler, S., P. Knippertz, S. Woodward, G. Martin, N. Bellouin, A. Ross, B. Heinold, K. Schepanski, C. Birch, and I. Tegen, A process-based evaluation of dust-emitting winds in the CMIP5 simulation of HadGEM2-ES, Clim. Dyn.,1–24, doi:10.1007/s00382-015-

2635-9, 2015.

Gallisai, R., Peters, F., Volpe, G., Basart, S., and Baldasano, J. M.: Saharan Dust Deposition May Affect Phytoplankton Growth in the Mediterranean Sea at Ecological Time Scales, *PloS One*, *9*, e110762. doi:10.1371/journal.pone.0110762, 2014.

Ginoux, P., M. Chin, I. Tegen, J. M. Prospero, B. Holben, O. Dubovik, and Lin, S. J.: Sources and distributions of dust aerosols simulated with the GOCART model, *J. Geophys. Res.-Atmos.*, *106*(D17), 20255-20273, 2001.

Guerrero-Rascado, J. L., F. J. Olmo, I. Avilés-Rodríguez, F. Navas-Guzmán, D. Pérez-Ramírez, H. Lyamani, and Alados Arboledas, L.: Extreme Saharan dust event over the southern Iberian Peninsula in september 2007: active and passive remote sensing from surface and satellite, *Atmos. Chem. Phys.*, *9*(21), 8453-8469, doi=10.5194/acp-9-8453-2009, 2009.

Heinold, B., J. Helmert, O. Hellmuth, R. Wolke, A. Ansmann, B. Marticorena, B. Laurent, and Tegen, I.: Regional modeling of Saharan dust events using LM-MUSCAT: Model description and case studies, *Journal of Geophysical Research: Atmospheres*, *112*(D11), D11204, doi=10.1029/2006JD007443, 2007.

Heinold, B., P. Knippertz, J. H. Marsham, S. Fiedler, N. S. Dixon, K. Schepanski, B. Laurent, and Tegen, I.: The role of deep convection and nocturnal low-level jets for dust emission in summertime West Africa: Estimates from convection-permitting simulations, J. Geophys. Res. Atmos., 118, 4385–4400, doi:10.1002/jgrd.50402, 2013.

Holben, B. N., T. F. Eck, I. Slutsker, D. Tanre, J. P. Buis, A. Setzer, E. Vermote, J. A. Reagan, Y. J. Kaufman, T. Nakajima, F. Lavenu, I. Jankowiak, and Smirnov, A.: AERONET - A federated instrument network and data archive for aerosol characterization, *Remote Sens. Environ.*, *66*(1), 1-16, 1998.

Hsu, N. C., Tsay, S. C., King, M. D., and Herman, J. R.: Aerosol properties over brightreflecting source regions. *IEEE Transactions on Geoscience and Remote Sensing*, *42*, 557–569. doi:10.1109/TGRS.2004.824067, 2004.

Hsu, N. C., Tsay, S. C., King, M. D., and Herman, J. R.: Deep Blue retrievals of Asian aerosol properties during ACE-Asia. *IEEE Transactions on Geoscience and Remote Sensing*, *44*, 3180–3195. doi:10.1109/TGRS.2006.879540, 2006.

Huneeus, N., M. Schulz, Y. Balkanski, J. Griesfeller, J.A. Prospero, S. Kinne, S. Bauer, O. Boucher, M. Chin, F. Dentener, T. Diehl, R. Easter, D. Fillmore, S. Ghan, P. Ginoux, A. Grini, L. Horowitz, D. Koch, M. Krol, W. Landing, X. Liu, N. Mahowald, R. Miller, J.-J. Morcrette, G. Myhre, J.E. Penner, J. Perlwitz, P. Stier, T. Takemura, and Zender, C.: Global dust model intercomparison in AeroCom phase I, Atmos. Chem. Phys., 11, 7781–7816, doi:10.5194/acp-11-7781-2011, 2011.

Huneeus, N., O. Boucher, and Chevallier, F.: Atmospheric inversion of SO2 and primary aerosol emissions for the year 2010, *Atmos. Chem. Phys.*, *13*(13), 6555-6573, doi=10.5194/acp-13-6555-2013, 2013.

Iversen, J. D., and White, B. R.: Saltation threshold on Earth, Mars and Venus, *Sedimentology, 29*, 111-119, 1982.

Jickells, T. D., Z. S. An, K. K. Andersen, A. R. Baker, G. Bergametti, N. Brooks, J. J. Cao, P. W. Boyd, R. A. Duce, K. A. Hunter, H. Kawahata, N. Kubilay, J. laRoche, P. S. Liss, N. Mahowald, J. M. Prospero, A. J. Ridgwell, I. Tegen, and R. Torres (2005), Global iron connections between desert dust, ocean biogeochemistry, and climate, *Science*, *308*(5718), 67-71

Jiménez, E., C. Linares, D. Martínez, and J. Díaz (2010), Role of Saharan dust in the relationship between particulate matter and short-term daily mortality among the elderly in Madrid (Spain), *Science of The Total Environment*, *408*(23), 5729-5736, doi=http://dx.doi.org/10.1016/j.scitotenv.2010.08.049.

Kalenderski, S., G. Stenchikov, and C. Zhao (2013), Modeling a typical winter-time dust event over the Arabian Peninsula and the Red Sea, *Atmos. Chem. Phys.*, *13*(4), 1999-2014, doi=10.5194/acp-13-1999-2013.

Karanasiou, A., N. Moreno, T. Moreno, M. Viana, F. de Leeuw, and X. Querol (2012), Health effects from Sahara dust episodes in Europe: Literature review and research gaps, *Environ. Int.*, *47*(0), 107-114, doi=http://dx.doi.org/10.1016/j.envint.2012.06.012.

Kim, K. W., Y. J. Kim, and S. J. Oh (2001), Visibility impairment during Yellow Sand periods in the urban atmosphere of Kwangju, Korea, *Atmospheric Environment*, *35*(30), 5157-5167

Largeron, Y., F. Guichard, D. Bouniol, F. Couvreux, L. Kergoat, and B. Marticorena (2015), Can we use surface wind fields from meteorological reanalyses for Sahelian dust emission simulations? *Geophys. Res. Lett.*, 42, doi:10.1002/2014GL062938.

Mahowald, N. M., S. Engelstaedter, C. Luo, A. Sealy, P. Artaxo, C. Benitez-Nelson, S. Bonnet, Y. Chen, P. Y. Chuang, D. D. Cohen, F. Dulac, B. Herut, A. M. Johansen, N. Kubilay, R. Losno, W. Maenhaut, A. Paytan, J. A. Prospero, L. M. Shank, and R. L. Siefert (2009), Atmospheric Iron Deposition: Global Distribution, Variability, and Human Perturbations, *Annu. Rev. Mar. Sci.*, *1*, 245-278.

Marticorena, B., and G. Bergametti (1995), Modeling the atmospheric dust cycle: 1. Design of a soil-derived dust emission scheme, *Journal of Geophysical Research: Atmospheres*, *100*(D8), 16415-16430, doi=10.1029/95JD00690.

Menut, L. (2008), Sensitivity of hourly Saharan dust emissions to NCEP and ECMWF modeled wind speed, J. Geophys. Res., 113, D16201, doi:10.1029/2007JD009522.

Morcrette, J. J., A. Beljaars, A. Benedetti, L. Jones, and O. Boucher: Sea-salt and dust aerosols in the ECMWF IFS model, Geophys. Res. Lett., 35, L24813, doi:10.1029/2008GL036041, 2008.

Morcrette, J. J., O. Boucher, L. Jones, D. Salmond, P. Bechtold, A. Beljaars, A. Benedetti, A. Bonet, J. W. Kaiser, M. Razinger, M. Schulz, S. Serrar, A. J. Simmons, M. Sofiev, M. Suttie, A. M. Tompkins, and A. Untch: Aerosol analysis and forecast in the European Centre for Medium-Range Weather Forecasts Integrated Forecast System: Forward modeling, J. Geophys. Res.-Atmos., 114, D06206, doi: 10.1029/2008JD011235, 2009.

Nickovic, S., G. Kallos, A. Papadopoulos, and O. Kakaliagou (2001), A model for prediction of desert dust cycle in the atmosphere, *Journal of Geophysical Research: Atmospheres*, *106*(D16), 18113-18129, doi=10.1029/2000JD900794.

Ozer, P., M. Laghdaf, S. O. M. Lemine, and J. Gassani (2007), Estimation of air quality degradation due to Saharan dust at Nouakchott, Mauritania, from horizontal visibility data, *Water Air and Soil Pollution*, *178*(1-4), 79-87.

Pérez, C., Nickovic, S., Pejanovic, G., Baldasano, J.M., Özsoy, E. (2006a), Interactive dust-radiation modeling: a step to improve weather forecast. *Journal of Geophysical Research*, 111, D16206. doi:10.1029/2005JD006717.

Pérez, C., S. Nickovic, J. M. Baldasano, M. Sicard, F. Rocadenbosch, and V. E. Cachorro (2006b), A long Saharan dust event over the western Mediterranean: Lidar, Sun photometer observations, and regional dust modeling, *Journal of Geophysical Research: Atmospheres*, *111*(D15), D15214, doi=10.1029/2005JD006579.

Pérez, C., K. Haustein, Z. Janjic, O. Jorba, N. Huneeus, J. M. Baldasano, T. Black, S. Basart, S. Nickovic, R. L. Miller, J. P. Perlwitz, M. Schulz, and M. Thomson (2011), Atmospheric dust modeling from meso to global scales with the online NMMB/BSC-Dust model - Part 1: Model description, annual simulations and evaluation, *Atmos. Chem. Phys.*, *11*(24), 13001-13027, doi=10.5194/acp-11-13001-2011.

Pérez García-Pando, C., Stanton, M., Diggle, P., Trzaska, S., Miller, R. L., Perlwitz, J. P., Baldasano, J. M., Cuevas, E., Ceccato, P., Yaka, P., and Thomson, M. (2014a). Soil dust aerosols and wind as predictors of seasonal meningitis incidence in niger. *Environmental Health Perspectives*, *122*, 679–686. doi:10.1289/ehp.1306640.

Pérez García-Pando, C., M.C. Thomson, M. Stanton, P. Diggle, T. Hopson, R. Pandya, and R.L. Miller (2014b): Meningitis and climate: From science to practice. Earth Perspectives., 1, 14, doi:10.1186/2194-6434-1-14.

Pey, J., X. Querol, A. Alastuey, F. Forastiere, and M. Stafoggia (2013), African dust outbreaks over the Mediterranean Basin during 2001-2011: PM10 concentrations, phenomenology and trends, and its relation with synoptic and mesoscale meteorology, *Atmos. Chem. Phys.*, *13*(3), 1395-1410, doi=10.5194/acp-13-1395-2013.

Querol, X., J. Pey, M. Pandolfi, A. Alastuey, M. Cusack, N. Pérez, T. Moreno, M. Viana, N. Mihalopoulos, G. Kallos, and S. Kleanthous (2009), African dust contributions to mean ambient PM10 mass-levels across the Mediterranean Basin, *Atmospheric Environment*, *43*(28), 4266-4277, doi=http://dx.doi.org/10.1016/j.atmosenv.2009.06.013.

Reid, J. S., A. Benedetti, P. R. Colarco, and Hansen, J. A.: International Operational Aerosol Observability Workshop, *Bull. Amer. Meteorol. Soc.*, *92*, ES21-ES24, doi=10.1175/2010bams3183.1, 2011.

Remer, L. A., Y. J. Kaufman, D. Tanre, S. Mattoo, D. A. Chu, J. V. Martins, R. R. Li, C. Ichoku, R. C. Levy, R. G. Kleidman, T. F. Eck, E. Vermote, and B. N. Holben (2005), The MODIS aerosol algorithm, products, and validation, *Journal of the Atmospheric Sciences*, *62*(4), 947-973.

Rienecker, M. M., Suarez, M. J., Gelaro, R., Todling, R., Bacmeister, J., Liu, E., Bosilovich, M. G., Schubert, S. D., Takacs, L., Kim, G.-K., Bloom, S., Chen, J., Collins, D., Conaty, A., da Silva, A, Gu, W., Joiner, J., Koster, R. D., Lucchesi, R., Molod, A., Owens, T., Pawson, S., Pegion, P., Redder, C. R., Reichle, R., Robertson, F. R., Ruddick, A. G., Sienkiewicz, M., and Woollen, J.: MERRA: NASA's Modern-Era Retrospective

Analysis for Research and Applications**.** *J. Climate*, 24, 3624-3648, doi:10.1175/JCLI-D-11-00015.1, 2011.

Ryder, C. L., Highwood, E. J., Rosenberg, P. D., Trembath, J., Brooke, J. K., Bart, M., … Washington, R. (2013). Optical properties of Saharan dust aerosol and contribution from the coarse mode as measured during the Fennec 2011 aircraft campaign. Atmospheric Chemistry and Physics, 13(1), 303–325. doi:10.5194/acp-13-303-2013

Sandu I, Beljaars A, Bechtold P, Mauritsen T, Balsamo G, Why is it so difficult to represent stably stratified conditions in numerical weather prediction (NWP) models? (2013), Journal of Advances in Modeling Earth Systems DOI 10.1002/jame.20013, URL http://dx.doi.org/10.1002/jame.20013.

Schroedter-Homscheidt, M., Oumbe, A., Benedetti, A., & Morcrette, J.-J. (2013). Aerosols for Concentrating Solar Electricity Production Forecasts: Requirement Quantification and ECMWF/MACC Aerosol Forecast Assessment. *Bulletin of the American Meteorological Society*, *94*(6), 903–914. doi:10.1175/BAMS-D-11-00259.1.

Schulz, M., Prospero, J. M., Baker, A. R., Dentener, F., Ickes, L., Liss, P. S., Mahowald, N. M., Nickovic, S., Pérez, C., Rodríguez, S., Manmohan Sarin, M., Tegen, I., and Duce, R. A., (2012). Atmospheric transport and deposition of mineral dust to the ocean: implications for research needs. *Environmental Science & Technology*, *46*, 10390–404. doi:10.1021/es300073u.

Shao, Y., Raupach, M. R., and Findlater, P. A.: Effect of saltation bombardment on the entrainment of dust by wind. *J. Geophys. Res.*, 98, 12719-12726 doi:10.1029/93JD00396, 1993.

Shao, Y., Y. Yang, J. Wang, Z. Song, L. M. Leslie, C. Dong, Z. Zhang, Z. Lin, Y. Kanai, S. Yabuki, and Chun, Y.: Northeast Asian dust storms: Real-time numerical prediction and validation, *Journal of Geophysical Research: Atmospheres*, *108*, 4691, doi=10.1029/2003JD003667, 2003.

Sokolik, I. N., D. M. Winker, G. Bergametti, D. A. Gillette, G. Carmichael, Y. J. Kaufman, L. Gomes, L. Schuetz, and J. E. Penner (2001), Introduction to special section: Outstanding problems in quantifying the radiative impacts of mineral dust, *J. Geophys. Res.-Atmos.*, *106*(D16), 18015-18027

Tegen, I. (2003), Modeling the mineral dust aerosol cycle in the climate system, *Quaternary Science Reviews*, *22*(18-19), 1821-1834

Terradellas, E., Baldasano, J.M., Cuevas, E., Basart, S., Huneeus, N., Camino, C., Dundar, C., and Benincasa, F.: Evaluation of atmospheric dust prediction models using ground-based observations, in: EGU General Assembly Conference, 7–12 April 2013, Vienna, Austria, Abstracts, Vol. 15, p. 8274, 2013.

Textor, C., M. Schulz, S. Guibert, S. Kinne, Y. Balkanski, S. Bauer, T. Berntsen, T. Berglen, O. Boucher, M. Chin, F. Dentener, T. Diehl, R. Easter, H. Feichter, D. Fillmore, S. Ghan, P. Ginoux, S. Gong, J. E. Kristjansson, M. Krol, A. Lauer, J. F. Lamarque, X. Liu, V. Montanaro, G. Myhre, J. Penner, G. Pitari, S. Reddy, O. Seland, P. Stier, T. Takemura, and X. Tie (2006), Analysis and quantification of the diversities of aerosol life cycles within AeroCom, *Atmos. Chem. Phys.*, *6*, 1777-1813

Vogel, B., Vogel, H., Bäumer, D., Bangert, M., Lundgren, K., Rinke, R., and Stanelle, T. (2009), The comprehensive model system COSMO-ART – Radiative impact of aerosol on the state of the atmosphere on the regional scale, Atmos. Chem. Phys., 9, 8661-8680, doi:10.5194/acp-9-8661-2009.

Washington, R., Flamant, C., Parker, D. J., Marsham, J., McQuaid, J. B., Brindley, H., Todd, M., Highwood, E. J., Chaboureau, J.-P., Kocha, C., Bechir, M., Saci, A., and Ryder, C. L. (2013), Fennec –The Saharan Climate System, submitted to CLIVAR Exchanges.

Winker, D. M., M. A. Vaughan, A. Omar, Y. Hu, K. A. Powell, Z. Liu, W. H. Hunt, and S. A. Young (2009), Overview of the CALIPSO Mission and CALIOP Data Processing Algorithms, *Journal of Atmospheric and Oceanic Technology*, *26*(11), 2310-2323, doi=10.1175/2009jtecha1281.1.

Woodward, S. (2001), Modeling the atmospheric life cycle and radiative impact of mineral dust in the Hadley Centre climate model, *Journal of Geophysical Research: Atmospheres*, *106*(D16), 18155-18166, doi=10.1029/2000JD900795.

Woodward, S. (2011), Mineral dust in HadGEM2, Hadley Centre Technical, Note 87, Met Office Hadley Centre, Exeter, Devon, UK.

Zhou, C. H., S. L. Gong, X. Y. Zhang, Y. Q. Wang, T. Niu, H. L. Liu, T. L. Zhao, Y. Q. Yang, and Q. Hou (2008), Development and evaluation of an operational SDS forecasting system for East Asia: CUACE/Dust, *Atmos. Chem. Phys.*, *8*(4), 787-798, doi=10.5194/acp-8-787-2008.

Dust model	Domain	Meteo. initial fields	Texture and vegetation type datasets	Radiation Interaction with dust	Horiz./Vert. resolution	Dust Emission Scheme	Surface wind speed for dust emission	Threshold friction velocity	Dry and wet deposition	Transport size bins
BSC-DREAM8b	Regional	NCEP	STATSGO-FAO 5 min USGS 1 km	P06	0.3°x0.3° 24 σ-layers	S93	viscous sublayer	B41 F99	Z01 N01	8 bins 0.1-10μm
NMMB/BSC-Dust	Regional/	NCEP	STATSGO-FAO 5 min USGS 1 km	no	0.25°x0.25° 40 σ-layers	W79-MB95	viscous sublayer	IW82 F99	Z01 BMJ	8 bins 0.1-10μm
ECMWF/MACC	Global	ECMWF	USGS 1km	no	1°x1° 91 layers	GP88-G01	10m gusts from 10m wind field	G01	B02 GC86	3 bins 0.03-20μm
MetUM™	Global	MetUM	FOA 2009	no	0.35°x0.23° 70 layers	W01, W11	10m wind field	B41 F99	W01	2 bins 0.1-10μm
DREAM8-NMME	Regional	ECMWF	STATSGO-FAO 5 min USGS 1 km	no	0.2°x0.2° 28 σ-layers	S93	viscous sublayer	B41 F99	Z01 N01	8 bins 0.1-10μm

Table 1 : Summary of the main features of each model included in the present contribution.

The codes denote the following references. B02: Boucher et al. (2002); B41: Bagnold (1941); F99: Fécan et al. (1999); G01: Ginoux et al. (2001); GC86: Giorgi and Chameides (1986); GP88: Gillette and Passi (1988); IW82: Iversen and White (1982); MB95: Marticorena and Bergametti (1995); S93: adapted Shao et al. (1993), P06: Pérez et al. (2006a); White (1979); Z01: Zhang et al. (2001); N01: Nickovic et al. (2001); W01: Woodward (2001); W11: Woodward (2011).

	Southern Europe			Central Europe			Northern Europe		
	24	48	72	24	48	72	24	48	72
DREAM8-NMME	0,18	0,21	0,18	0,13	0,14	0,15	0,19	0,19	0,20
BSC-DREAM8b	0,20	0,20	0,19	0,17	0,17	0,16	0,32	0,33	0,31
ECMWF/MACC-Dust	0,18	0,17	0,24	0,15	0,14	0,14	0,12	0,18	0,12
NMMB_BSC	0,19	0,21	0,23	0,17	0,16	0,17	0,23	0,26	0,25
MetUM	0,12	0,14	0,14	0,15	0,16	0,15	0,18	0,18	0,24

Table 2: Root mean square (RMS) error quantifying the performance to reproduce AERONET total AOD for each model. The statistics are computed for stations in Southern, Central and Northern Europe (Fig. 1), considering the period between the 5th and 11th of April. We note that for all models the dust AOD was used.

	Southern Europe			Central Europe			Northern Europe		
	24	48	72	24hr	48	72	24hr	48	72
DREAM8-NMME	-0,10	-0,10	-0,09	-0,06	-0,06	-0,06	-0,06	-0,07	-0,06
BSC-DREAM8b	-0,09	-0,10	-0,08	-0,10	-0,10	-0,08	-0,22	-0,22	-0,20
ECMWF/MACC-Dust	0,09	0,07	0,08	-0,07	-0,07	-0,06	-0,06	-0,07	-0,05
NMMB_BSC	-0,11	-0,11	-0,08	-0,10	-0,10	-0,10	-0,13	-0,15	-0,11
MetUM	0,04	0,06	0,02	-0,06	-0,06	-0,04	-0,03	-0,04	-0,03

Table 3: Same as Table 2 but for mean bias (MB).

	Southern Europe			Central Europe			Northern Europe		
	24	48	72	24hr	48	72	24hr	48	72
DREAM8-NMME	0,76	0,62	0,74	0,50	0,42	0,21	0,74	0,75	0,67
BSC-DREAM8b	0,66	0,66	0,66	0,17	0,11	0,04	0,64	0,63	0,48
ECMWF/MACC-Dust	0,83	0,81	0,69	0,29	0,37	0,41	0,91	0,78	0,91
NMMB_BSC	0,72	0,64	0,61	0,14	0,24	0,11	0,76	0,54	0,47
MetUM	0,89	0,87	0,81	0,20	0,12	0,17	0,72	0,73	0,43

Table 4: Same as Table 2 but for Pearson correlation coefficient (R).

	RMS			Mean Bias			Correlation		
	24	48	72	24	48	72	24	48	72
DREAM8-NMME	15,9	17,1	16,6	-0,4	-2,1	-1,8	0,22	0,13	0,15
BSC-DREAM8b	28,6	27,3	28,8	12,0	11,7	12,7	0,38	0,41	0,35
ECMWF/MACC-Dust	28,1	28,9	28,6	20,2	20,7	20,1	0,36	0,34	0,47
NMMB_BSC	16,8	16,0	15,2	-9,9	-9,6	-7,6	0,46	0,55	0,53
MetUM	147,1	126,5	125,1	110,7	99,0	100,4	0,29	0,35	0,38

Table 5: Root mean square (RMS) error, mean bias and correlation quantifying the performance to reproduce dust surface concentration in the Iberian Peninsula. Figure 1 illustrates the location of the stations used in the computation of the statistics. We note that for the models, the total dust surface concentration was used.

	AOD			Sfc. Conc.		
	24	48	72	24	48	72
DREAM8-NMME	0,35	0,37	0,34	1,06	0,99	0,98
BSC-DREAM8b	0,41	0,44	0,43	1,91	1,86	1,88
ECMWF/MACC-Dust	0,50	0,50	0,62	2,28	2,36	1,96
NMMB_BSC	0,45	0,48	0,48	0,75	0,67	0,71
MetUM	0,34	0,39	0,38	9,75	8,70	8,78

Table 6: Mean normalized gross error quantifying the performance to reproduce AERONET total AOD in Southern Europe and surface concentration for each model and each lead-time forecast. We note that for the models, the dust AOD and dust total surface concentrations were used.

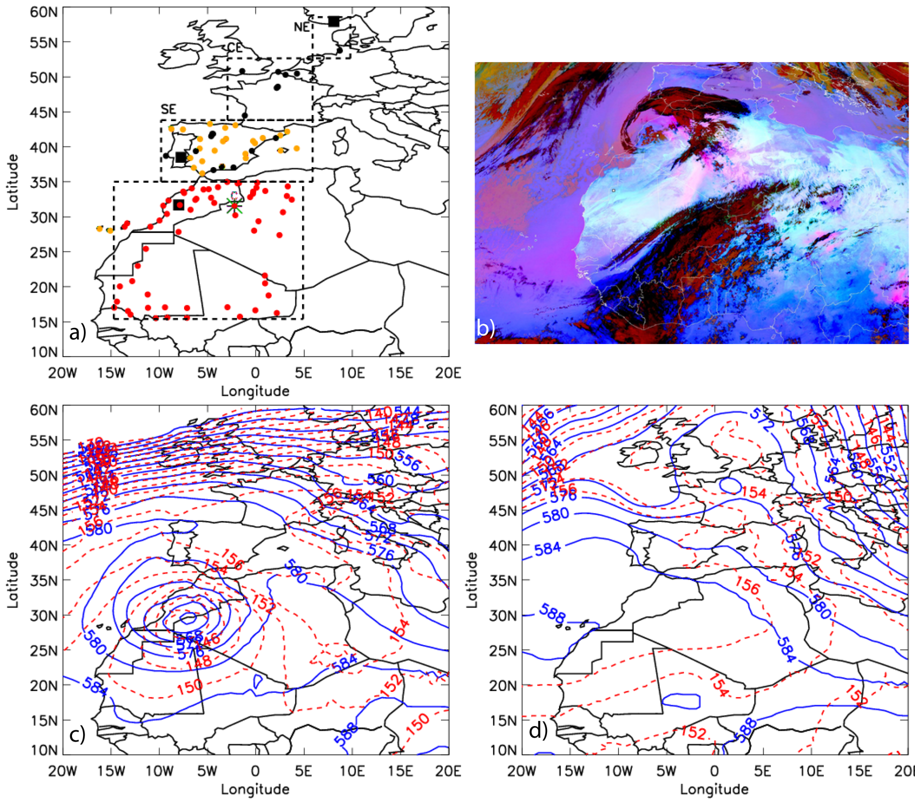

Figure 1: (a) AERONET (orange), surface concentration (black), surface wind (green) and radiosounding (brown) stations used in this study are presented. Southern, Central and Northern Europe (SE, CE and NE, respectively as the dashed black squares) regions used in the statistical analysis are illustrated, as well as the region used to produce the emission time series in Figure 5. (b) The MSG/RGB dust product of the "spinning enhanced visible and infrared imager" (SEVIRI) shows the cloud band of the cyclone (red) and dust aerosol (pink) of the dust event over Northwest Africa on 5th April 2011 at 12:00. (c) Geopotential height at 500 hPa (blue lines) and (d) 850 hPa (red lines) for the 5th and 10th of April 2011 and wind field at 850 hPa.

Figure 2: Total AOD at 550 nm at three selected sites from the AERONET network (blue line) and 24 (first row), 48 (second row) and 72 hr (third row) forecast of the model MetUM (red), ECMWF/MACC (green), BSC-DREAM8b (brown), NMMB/BSC-Dust (orange) and DREAM8-NMME (purple) are illustrated. The Angström exponent (dark blue dots) from the AERONET network at the three selected sites is included in the forth row. Angström exponent <0.75 indicate the dominance of desert dust.

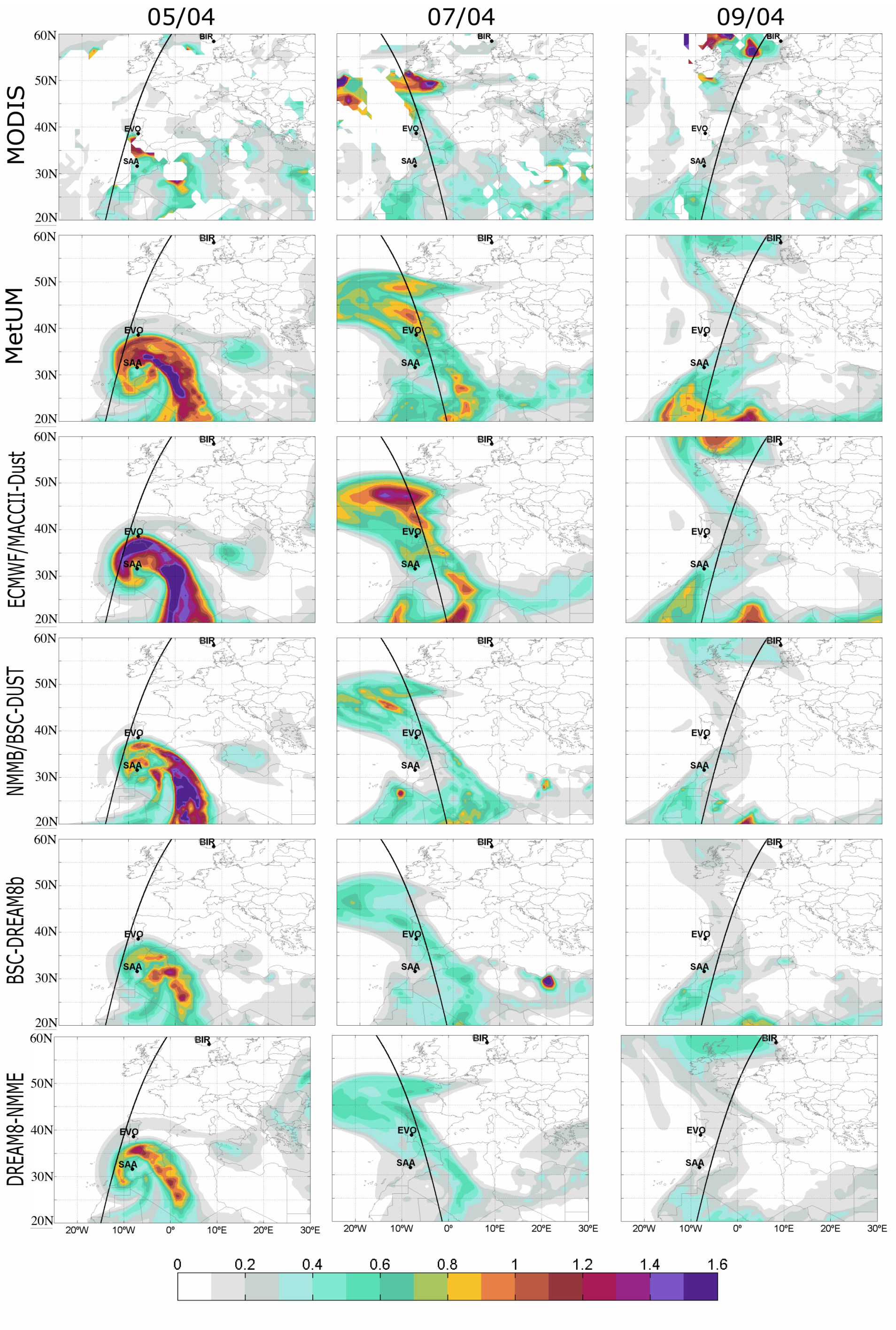

Figure 3: Maps of daily total AOD at 550 nm from MODIS (first row) and corresponding 24-hour forecast of models MetUM (second row), ECMWF/MACC (third row), NMMB/BSC-DUST (fourth row), BSC-DREAM8b (fifth row) and DREAM8-NMME (sixth row) for the 5th (first column), 7th (second column) and 9th (third column) of April 2011. Corresponding maps for all days between 4th and 11th of April are given in Figure S01 in the Supplement and 48 and 72-hour forecast maps are provided in Figure S02 and S03. The three AERONET site show in Fig. 2 (black dots) and the CALIPSO orbits (black lines) are also shown. The simulated AOD is computed as the average of the fields at 12 and 15 UTC.

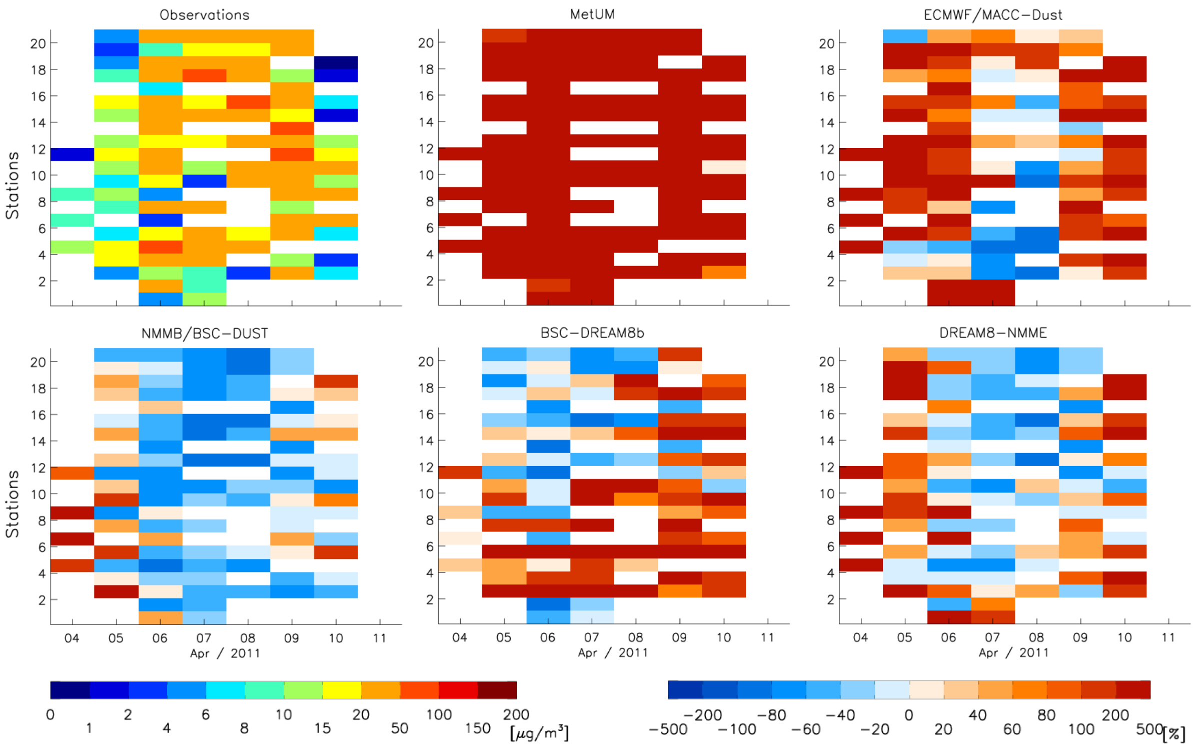

Figure 4: Daily measured surface concentration [μg m^{-3}] and normalized bias of corresponding 24 hour forecast surface concentration [%] at stations illustrated in Figure 1. Each row corresponds to one of the stations. Stations are ordered from south to north and white colour corresponds to days without measurements. Corresponding 24-hour forecast model surface concentration are illustrated in Figure S04 in the Supplement and the 48 and 72-hour of normalized bias of forecasted surface concentration are provided in Figure S05 and S06.

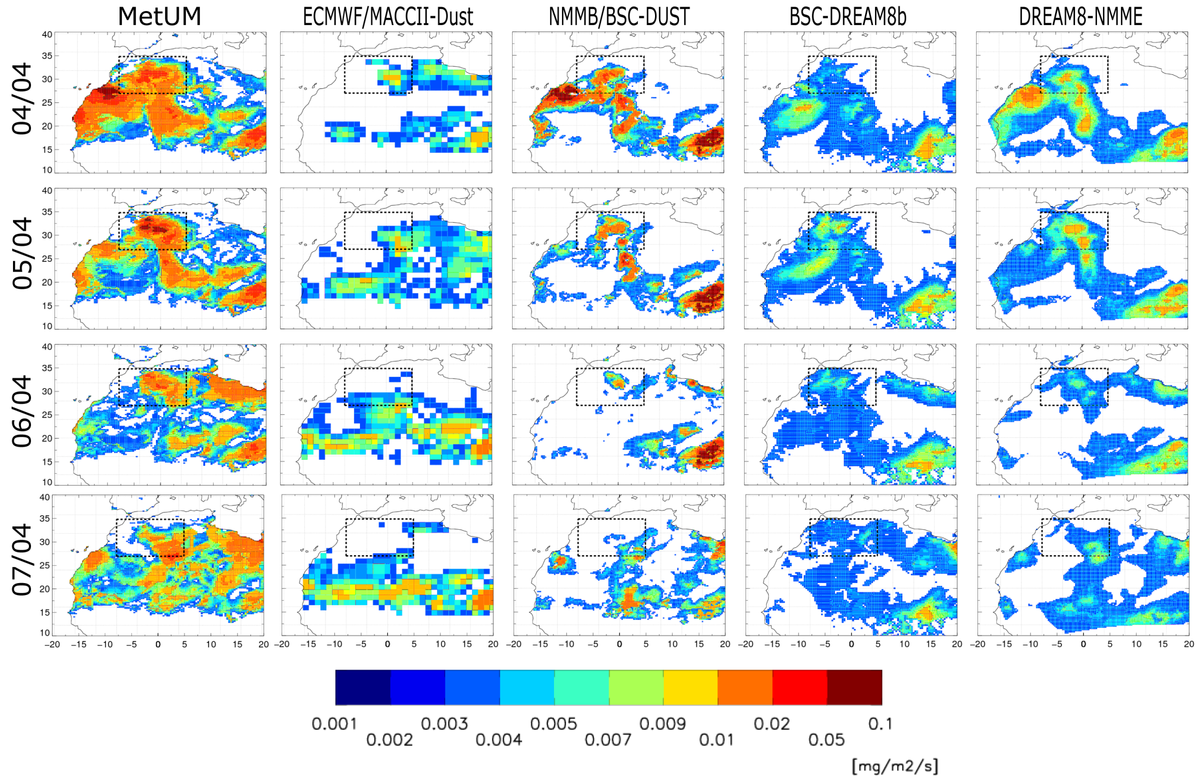

Figure 5: Forecasted daily average emission with 24-hour lead-time for the models MetUM (first column), ECMWF/MACC (second column), NMMB/BSC-DUST (third row), BSC-DREAM8b (forth column) and DREAM8-NMME (fifth row). Dashed box illustrates region used in the time series emissions illustrated in Figure 6.

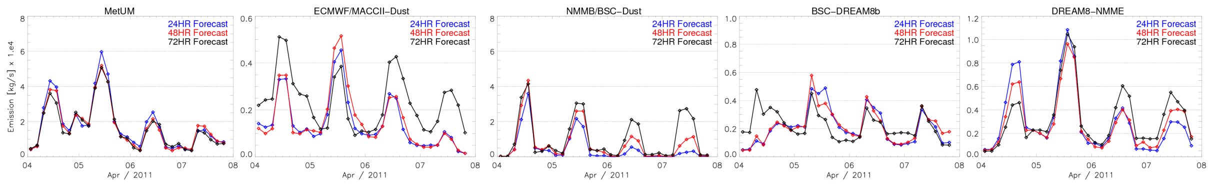

Figure 6: Time series of 3 hourly emissions from models MetUM^{TM}, ECMWF/MACC, NMMB/BSC-Dust, BSC-DREAM8b and DREAM8-NMME with 24, 48 and 72 hours lead-time (blue, red and black respectively).

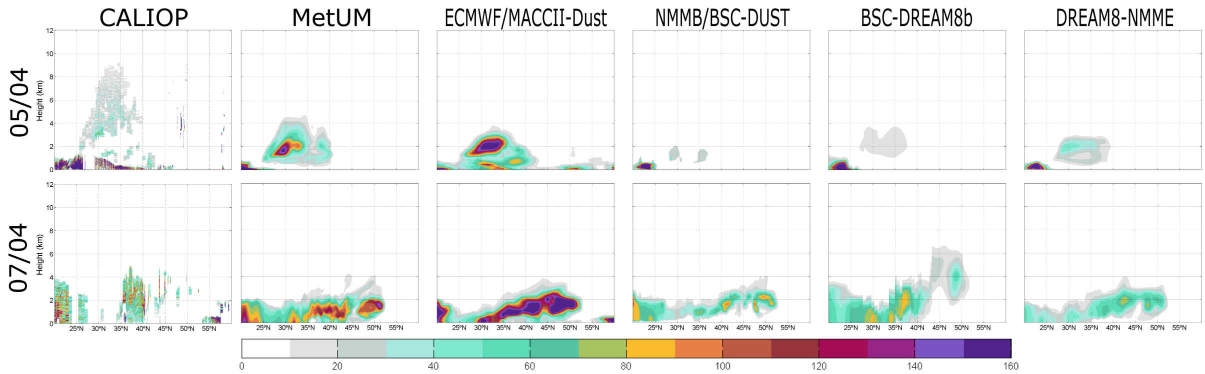

Figure 7: Profiles of measured total extinction coefficient at 532 nm from the CALIOP instrument onboard of the CALIPSO satellite and 24 hour forecasted dust extinction coefficient profiles at 532 nm from models MetUM, ECMWF/MACC, NMMB/BSC-DUST, BSC-DREAM8b and DREAM8-NMME. Conditions are presented for the 5th (upper row) and 7th (lower row) of April. Overpass of the satellite in each case is illustrated in Figure 3. Corresponding forecasted model profiles for 48 and 72 hours lead times are illustrated in Figure S10 and S11, respectively)

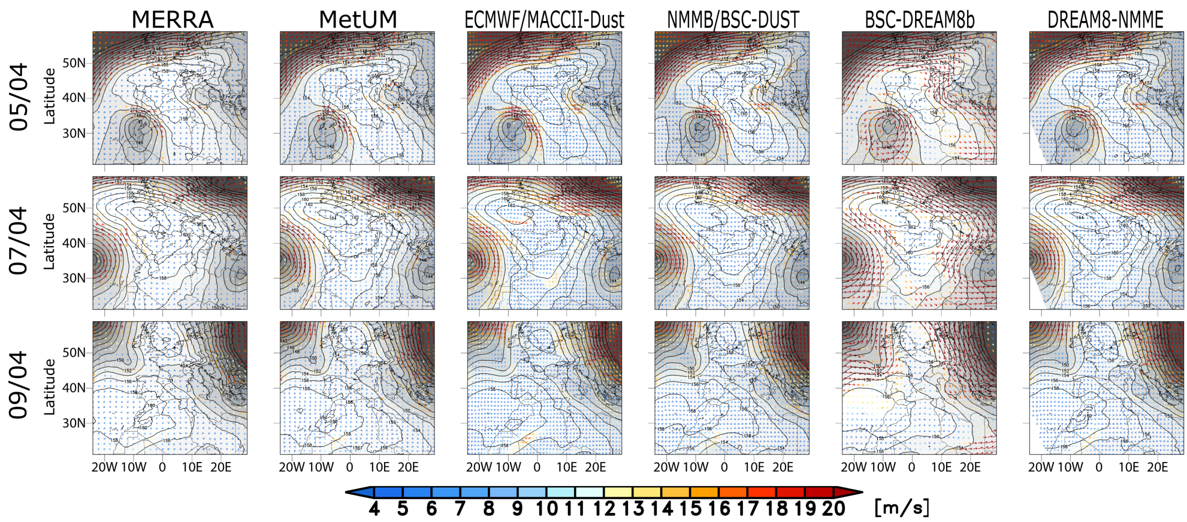

Figure 8: The geopotential height (grey shaded with contour labels in gpdm) and wind speed stream lines at 850 hPa on 5th (first row), 7th (second row) and 9th (third row) of April 2011 at 12 UTC from MERRA reanalysis and the 24 hour forecast from MetUM, ECMWF/MACC, NMMB/BSC-DUST, BSC-DREAM8b and DREAM8-NMME (from left to right).

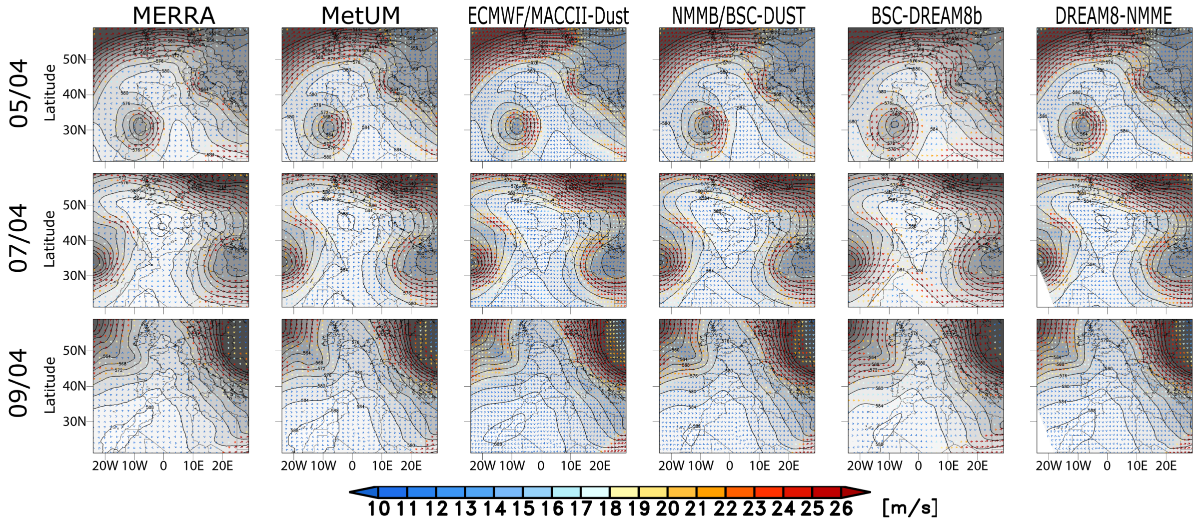

Figure 9: Same as Figure 8 but for 500 hPa.

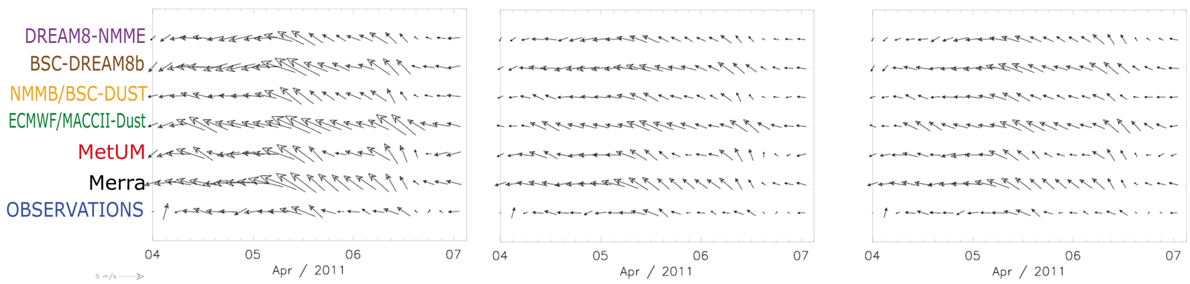

Figure 10: Time series of near-surface wind speeds in dust source region. Three-hourly values of the 10m-wind speed from observations and re-analysis (MERRA), global models and regional models for the period 4 Apr 2011 to 7 Apr 2011 with (a) 24 hours lead time, (b) 48 hours, and (c) 72 hours. Observations are averaged over the region illustrated in Figure 1. The 10m-winds from the models are averaged over the grid boxes enclosing the observation station.

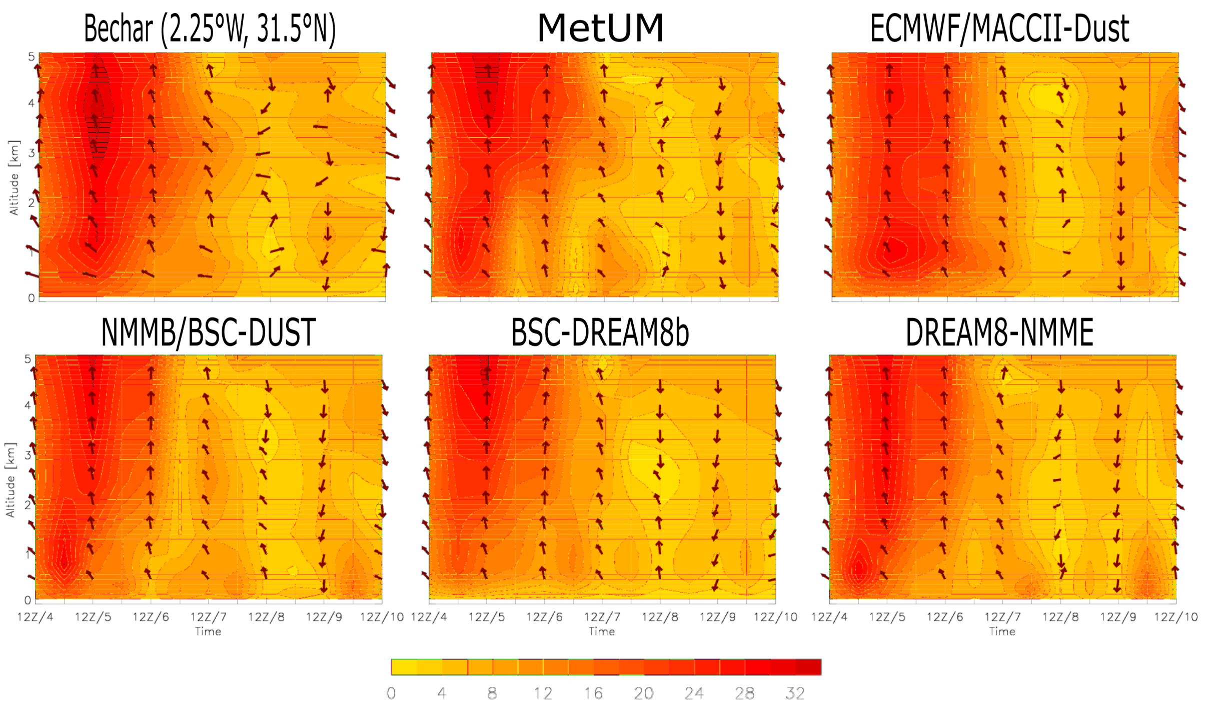

Figure 11: Profiles of measured wind speed (m/s, filled contours) and direction (vectors, first column) between the 4th and 10th of April from radiosounding at Bachar (2.25°W, 31.5°N; first row) and the corresponding 24-hour forecast of models MetUM, ECMWF/MACC, NMMB/BSC-DUST, BSC-DREAM8b and DREAM8-NMME.

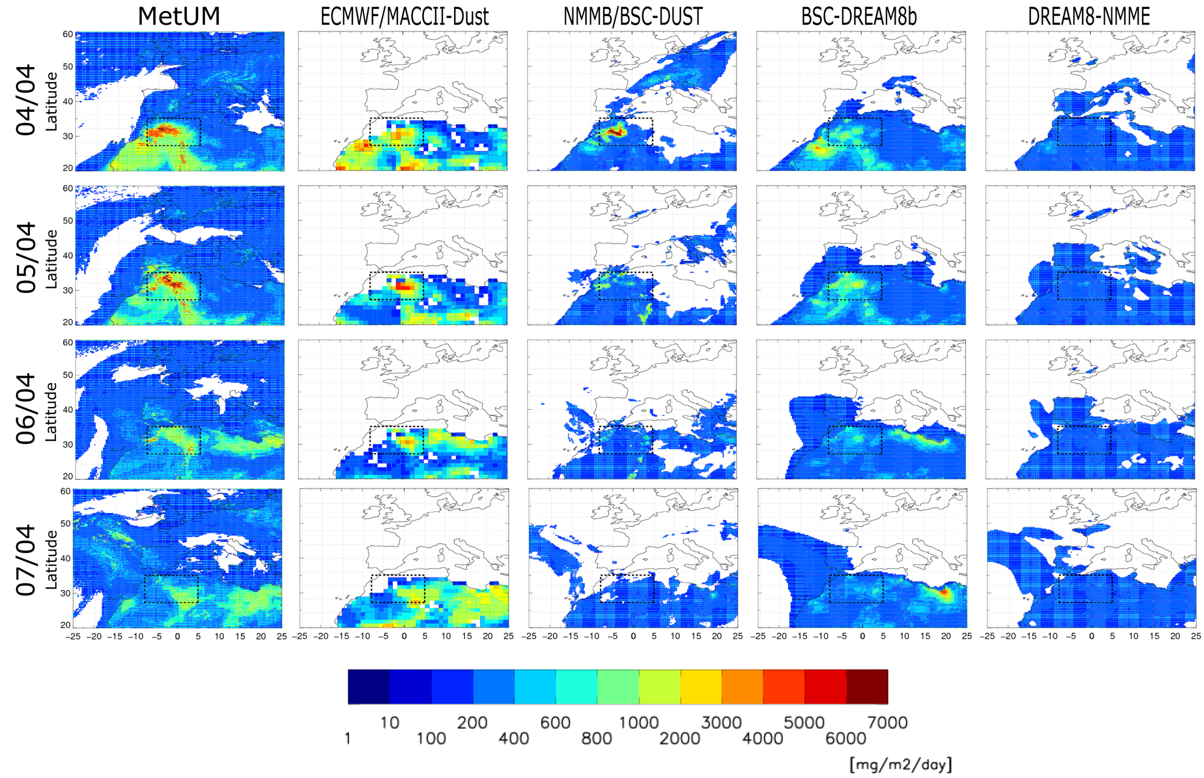

1042

1043 **Figure 12:** Total accumulated forecasted daily deposition with 24-hour lead time for the models MetUM,

1044 ECMWF/MACCII-Dust, NMMB/BSC-DUST, BSC-DREAM8b and DREAM8-NMME (from left to right).